Infrared Evidence of a Third Brønsted Site in Mordenites

Olivier Marie,*,† Pascale Massiani,‡ and Frédéric Thibault-Starzyk†,§

Laboratoire Catalyse & Spectrochimie, CNRS-ENSICAEN, 6 Bd du Maréchal Juin, 14050 Caen Cedex, France, Laboratoire de Réactivité de Surface, CNRS-UPMC, 4 place Jussieu, casier 178, 75252 Paris Cedex 05, France, and Churchill College, Cambridge CB3 0DS, United Kingdom

Received: December 18, 2003; In Final Form: February 13, 2004

A series of progressively proton-exchanged sodium mordenite was studied by FTIR spectroscopy in the presence of probe molecules to precise the location of protons and sodium ions in the structure of MOR. The atomic ratio between protons in unconstrained and constrained environments in fully exchanged mordenite was 2:1 as shown by the adsorption of both pyridine and CO. On the contrary, this ratio was 1:2 for the Na^+ cations in the parent Na-mordenite as deduced from CO adsorption and from the formation of $NaNO_3$ in the structure by NO + O_2 reaction. Therefore, some framework Al atoms lead to unconstrained OH groups in the acidic form but to constrained Na^+ cations in the sodium form. This observation, the appearance of a new ν(OH) component at ca. 3605 cm^{-1}, and the quantitative infrared data at intermediate exchange levels allow to conclude that not only two but at least three different OH types can be distinguished by infrared spectroscopy in the MOR structure, in line with recent structural proposals. A model is proposed for the exchange process, in which the unconstrained OH environment classically reported on infrared basis can be split in two different sites.

1. Introduction

Mordenite is an important zeolitic system that is active and shape-selective in many refining and petrochemical catalytic processes.[1−6] It is particularly attractive on a structural point of view (MOR structure) because of its specific pore system which consists of large 12-membered rings (12-mr) main channels, with an elliptical shape of ca. 6.7 × 7.0 Å running along the *c* crystallographic axis, to which side pockets are connected in the *b* direction, formed by 8-membered rings (8-mr) with ca. 3.4 × 4.8 Å aperture.[7] This strongly interconnected large/small microporous system may generate important confinement effects, as was shown for ammonia[8] and acetonitrile adsorption,[9−10] and thus leads to specific active properties of the Brønsted acid sites. It was reported that protons in H-mordenite can display a greater initial activity in craking of *n*-hexane than in other zeolite types,[11] although acidity measurements gave no clear justification for it.[12] Similarly, H-mordenite is very active in the important application of xylenes isomerization, but the reasons for its high selectivity in disproportionation and transalkylation side reactions[1,13] are still unclear.[14] Indeed, these side reactions are favored by strong acid sites but they were significantly and surprisingly reduced by removing supposedly less acidic protons from the side pockets.[1,15−17] Acidity measurements by NH_3 TPD experiments suggested a higher effective acid strength for hydroxyls in the side pockets.[18−20]

Brønsted acid sites in zeolites are due to H^+ cations compensating the defect charges generated by the presence of tetrahedral Al atoms in the framework. They lead to specific ν(OH) vibration bands in the infrared spectra and this technique has long been used to identify the location and strength of Brønsted acid sites in zeolites. In H-mordenite, the ν(OH) band for acidic OH groups is usually rather broad and has an unusual low-frequency component.[16,21] This low-frequency component was perturbed by adsorption of NH_3[20] but not by adsorption of the bulkier benzene or cyclohexane molecules, suggesting that the relevant OH groups are located in the side pockets of the structure.[18] This assignment was later confirmed by the adsorption of pyridine,[16] C_6H_6, and cyclohexane.[21] The low-frequency ν(OH) vibration band is thus due to a strong interaction of the OH groups in the side pockets with neighboring oxygen atoms through H-bonding, in agreement with the pioneering work of Jacobs and Mortier who concluded that OH groups vibrating in 8-mr undergo a shift to lower wavenumbers when compared to the frequency at which their vibration would occur in the 12-mr[22] and with a recent study using nonlinear-infrared spectroscopy and pump−probe experiments.[23]

The high and low frequency assignment to OH groups in the main channels (OH_{MC}) and side pockets (OH_{SP}), respectively, is now classically admitted. However, three different cationic sites were determined for sodium cations in defect-free Na-mordenite samples[24] which implies three different locations for negative charge to compensate and one would thus expect similarly three different Brønsted acidic OH types in the structure of H-mordenite after exchange of the Na^+ cations by protons. To our knowledge, however, only a few recent publications so far report anything in that direction. On one hand, Bevilacqua et al. proposed from infrared studies on the adsorption of three nitriles with increasing molecular sizes that three different framework OH types may exist in acidic mordenite.[25] Nevertheless, their sample was dealuminated during activation so that defect sites and extraframework aluminum species were created which could strongly modify the sites distribution and accessibility. On the other hand, Alberti

* Address correspondence to this author. Tel/fax: +33 23145 2825/2822; e-mail: marieo@ismra.fr.
† Laboratoire Catalyse & Spectrochimie.
‡ Laboratoire de Réactivité de Surface.
§ Churchill College.

10.1021/jp037915v CCC: $27.50
Published on Web 03/30/2004

TABLE 1: Conditions of Preparation and Chemical Compositions of the Samples

sample name	m NH_4Cl (0.1N)/m Na-MOR	Na/Al[a] (mol/mol)	Si/Al[a] (mol/mol)	$H^+ = Al - Na$[a] (μmol/g_{cat}^{-1})	PyH^+ (μmol g_{cat}^{-1})[b]
H_0Na_{100}MOR	−	1	10.2	0	0
$H_{31}Na_{69}$MOR	3.5	0.69	10.2	400	395
$H_{72}Na_{28}$MOR	9.5	0.28	10.3	930	680
$H_{78}Na_{22}$MOR	12.4	0.22	10.2	1000	750
$H_{97}Na_3$MOR	100	0.03	10.2	1200	750
$H_{100}Na_0$MOR	75 (repeated 3 times)	0.007	10.4	1290	750

[a] From elemental chemical analyses. [b] From quantitative infrared studies in the presence of Py.

proposed from a cross-check of crystallochemical and spectroscopic bibliographic data that three[26] or even four[27] types of oxygen atoms can bear acidic protons in the MOR structure: two in the main channels and two in the side pockets. However, their samples were not only dealuminated by fast thermal treatment but also contained residual adsorbed water molecules which could perturb the OH sites distribution and accessibility.

Therefore, our aim in this work was to precise the number of Brønsted acid OH groups that can be distinguished by infrared spectroscopy in the zeolitic framework of dehydrated, nondealuminated defect-free mordenite. Using pyridine, CO, and NO^+ as probe species and a series of mordenite samples (with various H^+ and Na^+ cation contents), we were able to detect three different OH sites related to exchangeable cations. We propose a model for the progressive cationic exchange in the zeolite.

2. Experimental Section

Six mordenite samples with varying H^+ and Na^+ cationic contents were obtained by exchange of a parent sodium mordenite sample (from Tosoh Corp., Si/Al = 10.2) in a NH_4-Cl solution (0.1 N), followed by a mild thermal treatment at 723 K (decomposition of the NH_4^+ ions into NH_3 and H^+) performed in flowing N_2 (physicochemical characterizations) or in a vacuum (infrared studies, see below). Table 1 details the conditions of the NH_4^+-exchange and the chemical contents (Na/Al and Si/Al atomic ratios) for all six thermally activated H_xNa_{100-x}MOR samples, where x and $100 - x$ are the percentages of H^+ and Na^+ cations, respectively. Note that x is also the level of exchange (in %) of the Na^+ cations by protons.

Infrared spectra were recorded at room temperature and at liquid nitrogen temperature (77 K) with a Nicolet Magna 550 FTIR spectrometer. Previous to experiments, the self-supported wafers of NH_4^+-exchanged zeolites (2 cm^2, 5−10 mg) were placed in a quartz infrared cell and carefully activated by heating under vacuum for 10 h (0.5 K/min, 723 K, 10^{-3} Pa).

Analytical grade pyridine (denoted as Py) from Aldrich was used after water trapping with molecular sieve 3A. CO, NO, and O_2 (99% pure) were provided by Air Liquide and labeled ^{15}NO (98.5% pure) was from ONIA. All gases were purified by low-temperature distillation/trapping before use.

Pyridine adsorption was performed by successive introduction of well-known doses inside the infrared cell containing the previously activated wafer. After each dose of Py, the mordenite sample was heated at 443 K for 10 min to allow diffusion toward all accessible sites. Infrared spectra were recorded after each dose adsorption and after Py saturation (1.33 mbar at equilibrium) followed by evacuation at 443 K under dynamic vacuum to remove physisorbed species.

CO adsorption was performed at 77 K by successive introduction of well-known doses inside the low-temperature infrared cell containing the previously activated wafers. Infrared spectra were recorded 15 min after each CO dose adsorption to allow the diffusion inside the micropores.

NO^+ and nitrate formation was achieved by introducing at room temperature an initial equimolar mixture of NO and O_2 ($P_{initial\ total} = 2$ Torr) inside the cell containing the H_0Na_{100}MOR sample. The pressure drop inside the cell indicating the reaction evolution was measured by a 0.1 Pa pressure gauge and was stable after 1 h contact time.

Graphical representation and modeling on computer were made with the software Hyperchem 6 using crystallographic data from the atlas of zeolites.[7]

3. Results

3.1. Structural and Chemical Properties. The crystallinity of samples is of prime importance for any reasoning on the number and location of sites inside the zeolite framework. We have evidence that thermal treatment of a 10-mg wafer performed under vacuum any faster than 1 K/min damages the structure, alters accessibility of sites, and creates Lewis sites (whereas the neatly activated sample does not contain any). X-ray diffraction experiments undertaken before and after thermal treatment showed that all our samples were highly crystalline. In addition, textural analyses derived from nitrogen adsorption isotherms indicated that the mesoporous volume was always very low (<0.04 $cm^3\ g^{-1}$) and kept constant for all samples before and after our gentle thermal treatment.

To quantify the amount of framework aluminum, we registered the infrared spectra (diluted sample in KBr) in the range typical of framework vibrations (1300−500 cm^{-1}, not shown) and applied the empiric correlation between the ν(Al−O) structural vibration and the number of framework aluminum (Al^{IV}) per unit cell established by Gooaverts et al.[28] For all samples, we obtained atomic Si/Al^{IV} framework ratios of 11 ± 0.2 which is very close to the global atomic Si/Al ratios obtained by elemental analysis (Table 1). In other words, we can conclude that, after our thermal treatment, more than 95% of aluminum is kept in framework tetrahedral position. Only in some[27]Al MAS NMR experiments were we able to detect a very low amount of Al atoms in octahedral coordination, typical of extraframework Al species. This, however, occurred only after thermal treatments specific to the NMR experiments (in which the temperature control might have been less efficient) and parent H_0Na_{100}MOR was free of octahedral Al. Moreover, no Lewis sites were detected by pyridine adsorption in any other thermally activated sample, as will be shown below.

3.2. Infrared Spectra of the OH Groups. Figure 1 shows the evolution of the ν(OH) infrared band upon progressive exchange of the Na^+ cations by protons in the H_xNa_{100-x}MOR samples. For all samples, the absence of any signal in the 3670−3650 cm^{-1} range typical of extraframework Al species[25] showed again that no framework dealumination took place during thermal activation. The absence of any signal in the 3650−3550 cm^{-1} range for H_0Na_{100}MOR confirmed the absence of any proton in this parent material (Figure 1a). At low proton content, only one symmetrical high-frequency component centered at 3610 cm^{-1} was observed (Figure 1b) and the

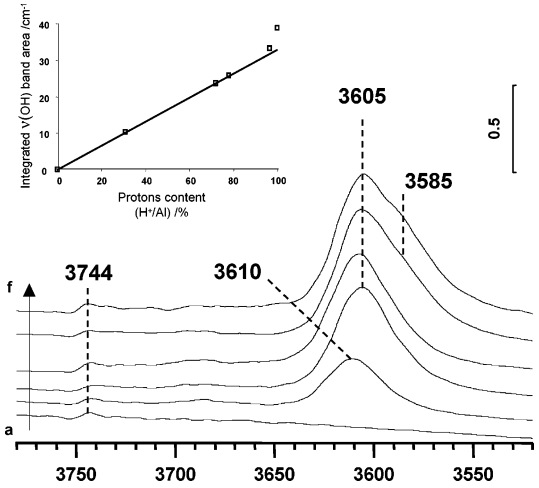

Figure 1. ν(OH) bands for thermally activated (a) H_0Na_{100}MOR, (b) $H_{31}Na_{69}$MOR, (c) $H_{72}Na_{28}$MOR, (d) $H_{78}Na_{22}$MOR, (e) $H_{97}Na_3$MOR, and (f) $H_{100}Na_0$MOR. Top left: progress of the integrated intensity of the ν(OH) vibration with the protons content.

intensity of the band increased when Na^+ substitution by H^+ went on, with simultaneous shift of the peak maximum toward lower wavenumbers (3605 cm^{-1}). At the highest exchange levels, one shoulder appeared around 3585 cm^{-1}, revealing that the spectra could possess three distinct components at ca. 3610, 3600−5, and 3585 cm^{-1} (Figure 1e, f). The first component at 3610 cm^{-1} is typical for OH_{MC} inside the main channels,[16,21] whereas the lower frequency component indicates confinement effects.[22−23] All spectra present a low intensity band at 3744 cm^{-1} which is due to terminal silanols (SiOH) stretching vibrations.

According to the Beer−Lambert law, the integrated area of an infrared absorption band in cm^{-1} is proportional to the number of active vibrators on the optical path. For powder solids, the optical path cannot be known accurately, and the wafer thickness is used instead, leading to $A(\nu) = \epsilon(\nu)\ Cd = \epsilon(\nu)\ n/S$, where $A(\nu)$ is the absorbance at ν wavenumbers, $\epsilon(\nu)$ is the corresponding molar absorption coefficient, C is the molar concentration, d is the wafer thickness, n is the number of active vibrators, and S is the surface of the wafer. This approximation was used extensively for quantitative infrared studies in heterogeneous catalysis and was recently shown to be valid even for strongly adsorbed probe molecules such as pyridine.[29] The inset in Figure 1 shows the integrated area of the ν(OH) bands as a function of the exchange level x in the H_xNa_{100-x}MOR samples. A straight line is obtained up to an exchange level of about 75% but a clear change in the slope is next detected, indicating that the absorption coefficient of the ν(OH) vibration band is higher for protons introduced at the end of the exchange process. Makarova et al.[21] gave evidence of an increase of $\epsilon(\nu)$ when ν(OH) vibrations are disturbed by the high electric field inside confined cavities, and they quantified the phenomenon for mordenite, $\epsilon(\nu)$ being 1.52 higher for OH_{SP} in the side pockets than for OH_{MC} in the main channels. In view of these data, the variation from the linear law observed for our samples indicates that the first steps of exchange lead to solely OH_{MC} acidic groups, followed at the highest exchange levels by the formation of the confined OH_{SP} acidic groups.

3.3. Pyridine Adsorption. Pyridine (Py, C_5H_5N) is a basic probe molecule widely used to characterize acidity in solids. It is particularly informative in mordenite since its molecular diameter (4.8 Å) prohibits the Py entrance in the side pockets (3.4 × 4.8 Å),[7] thus permitting acces to sites in the main channels only.[16]

Figure 2 reports the infrared spectra of our series of samples in the presence of adsorbed pyridine (the spectrum of proton-free H_0Na_{100}MOR is not shown). The overall spectra contain three typical regions (Figure 2A): the first one around 3600 cm^{-1} corresponds to ν(OH) stretching vibrations, the second one between 2800 and 3300 cm^{-1} is assigned to ν(CH) and ν(NH) vibration bands of adsorbed Py, and the last one, between 1400 and 1700 cm^{-1}, is the region of the νCC(N) vibration modes of the Py cycle. Detailed views are shown for the ν(OH) (Figure 2B) and νCC(N) (Figure 2C) vibration ranges.

The position of bands of the νCC(N) cycle vibrations gives information on the nature of the sites interacting with Py, allowing in particular discrimination between Brønsted and Lewis acid sites.[30−34] The three bands at 1490, 1545, and 1635 cm^{-1} observed for all of our proton-containing samples (Figure 2C) can be assigned to Py coordinated to protons but only that at 1545 cm^{-1} is typical for pyridinium ions, the two others being also possibly attributed to Py interacting with Lewis acid sites. Nevertheless, the interaction of Py with Lewis acid sites would also lead to a specific band at ca. 1450−55 cm^{-1}, depending on the acid strength,[33] but no such band could be detected for any of our H_xNa_{100-x}MOR samples. This confirms again the very low amount of extraframework aluminum species previously determined by the ν(Al−O) IR frequency, the 3670−3650 cm^{-1} OH range, and the ^{27}Al MAS NMR data. Moreover, no band around 1443 cm^{-1} characteristic of the interaction of Py with Na^+ cations (as determined by adsorption over H_0Na_{100}-MOR) was observed after heating in a vacuum. Thus, in all samples, pyridine is coordinated to only protons which allows quantification of the Brønsted acid sites accessible to the Py probe molecule.

At low exchange level, no more ν(OH) bands for Brønsted acidic OH can be observed in the 3650−3540 cm^{-1} range after Py adsorption (Figure 2B, a), confirming that the acid hydroxyls created during the first steps of exchange are all located in the large main channels where they can easily interact with Py. At the opposite, at high exchange levels, an intense signal at 3585 cm^{-1} persisted after Py adsorption (Figure 2B, d, e), supporting the attribution of this low frequency ν(OH) component to OH_{SP} groups in the side pockets, inaccessible to Py. This low frequency component was hardly detected at exchange levels as high as about 75% (Figure 2B, b, c), confirming that the OH_{SP} groups appear only at the last steps of the exchange process. Moreover, a new weak component around 3605 cm^{-1} could be identified in the presence of Py at this 75% proton contents, revealing that a third type of OH groups exists which is only partly accessible to Py and most probably located on an intermediate constrained site in view of its intermediate frequency.

The amount of Brønsted acid sites was estimated from the amount of adsorbed Py by assuming that one Py molecule interacts with one acid OH group. Figure 3 illustrates the introduction of successive Py doses in proton-rich $H_{97}Na_3$MOR. A good correlation was seen between the disappearance of the 3610 cm^{-1} infrared signal of OH_{MC} accessible to pyridine (Figure 3A) and the increase of the 1545 cm^{-1} band of pyridinium ions (Figure 3B). The plot of the integrated intensity of the 1545 cm^{-1} band versus the amount of Py introduced inside the cell is a linear curve up to the first ten Py doses illustrating the interaction of adsorbed Py molecules with Brønsted acid sites. This linear evolution is followed by a saturation plateau indicating the presence of physisorbed Py (Figure 3C). The slope of the linear curve was used to calculate the integrated molar extinction coefficient of the band of

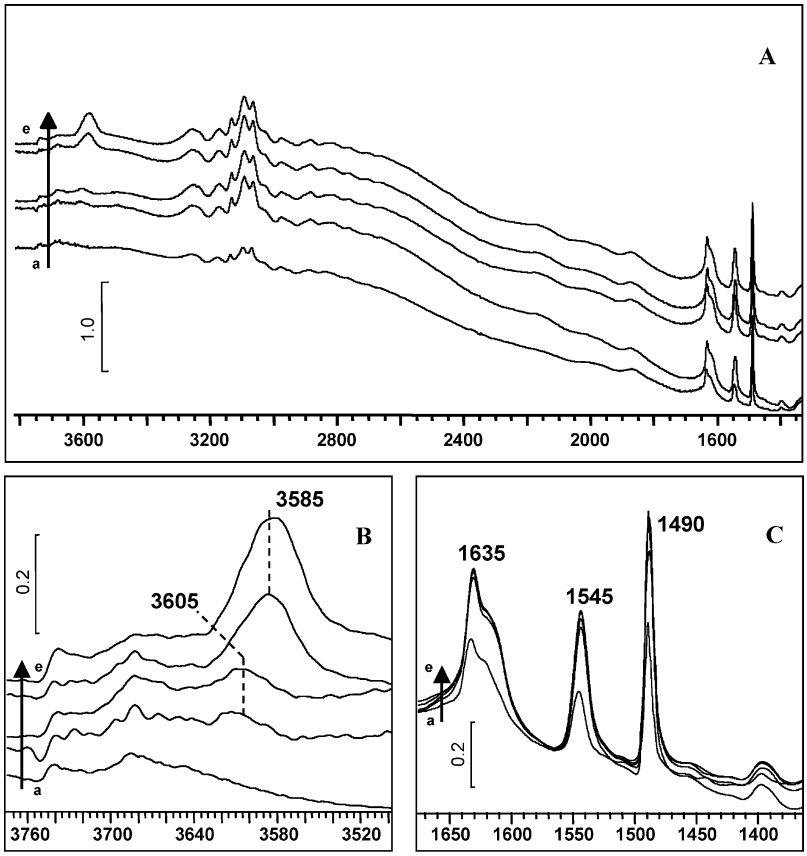

Figure 2. (A) Infrared spectra in the 3800−1400 cm^{-1} range of samples after pyridine saturation (1.33 mbar at equilibrium) and evacuation at 443 K: (a) $H_{31}Na_{69}MOR$; (b) $H_{72}Na_{28}MOR$; (c) $H_{78}Na_{22}MOR$; (d) $H_{97}Na_3MOR$; (e) $H_{100}Na_0MOR$. Enlargements in the (B) ν(OH) and (C) νCC(N) pyridine cycle vibration regions.

pyridinium ions (ϵ is the product of the slope of the straight line and the wafer area). The value obtained ($\epsilon = 1.8\ 10^6$ $cm.mol^{-1}$) fully agrees with previous literature data on mordenite[16] and faujasite.[35] Using this value and the 1545 cm^{-1} band integrated intensities after Py saturation and evacuation, we were able to determine the amounts of Brønsted acid sites accessible to Py in all $H_xNa_{100-x}MOR$ materials. The PyH^+ values thus obtained are listed in Table 1.

For $H_{31}Na_{69}MOR$ in which all hydroxyls are OH_{MC} accessible to Py, the PyH^+ value was in perfect agreement with the number of protons ($H^+ = Al-Na^+$) obtained from chemical analysis (Table 1). This proves the validity of our method for the determination of the number of Brønsted acid sites accessible to Py. However, at proton contents higher than about 40−50%, PyH^+ was always lower than the amount of protons given by chemical analysis (Figure 4). Therefore, some acidic hydroxyls were already inaccessible to Py at around 50% exchange level, although these groups cannot be OH_{SP} as these would only appear at exchange levels higher than 75%, as discussed above. This points again to the presence of some intermediate OH groups only partly accessible to Py. The total amount of hydroxyls calculated from Py adsorption kept increasing to around 80% proton content, where it stabilized, giving new evidence that the last H^+ to be formed is localized inside the side pockets. Finally, for $H_{100}Na_0MOR$, the experimental ratio $PyH^+/[Al-Na^+]$ was close to 2/3, revealing that two-thirds of the OH groups in fully acidic mordenite are accessible to Py, in line with previous estimations.[16,21]

3.4. CO Adsorption. The interaction of carbon monoxide (CO) with cations in zeolites leads to specific ν(CO) vibration bands that can be used to determine the cationic locations in the structure.[36] We performed the adsorption of CO on fully exchanged $H_{100}Na_0MOR$ (Figure 5A) and on parent H_0Na_{100}-MOR (Figure 5B) to precise the H^+ and Na^+ locations in the fully protonic and sodium forms of mordenite.

The adsorption of CO at saturation on $H_{100}Na_0MOR$ led to the complete disappearance of all free ν(OH) acidic bands (not shown), indicating that all acidic OH groups interact with the small CO probe molecule, including those inside the side pockets. In the ν(CO) vibration range, the adsorption of CO on $H_{100}Na_0MOR$ (Figure 5A) gave rise to two bands centered at about 2180 and 2171 cm^{-1} at low coverage. These bands increased in intensity and slightly shifted toward lower wavenumbers (2177 and 2169 cm^{-1}, respectively) when CO adsorption went on. At 1.33 mbar CO equilibrium, they merged into a broader band with maximum at 2175 cm^{-1}. The blue shift of the ν(CO) vibration band from its gas-phase frequency (2143 cm^{-1}) is due to the acid−base interaction between the probe and the adsorption site: the stronger the interaction, the higher the corresponding ν(CO) wavenumber. The additional band around 2137 cm^{-1} at high CO coverage revealed the presence of physisorbed (pseudo-liquid) CO in the pores.[37] From pyridine and CO coadsorption experiments over mordenite, Maache et al. were able to isolate the specific interaction of CO with hydroxyls located inside the side pockets and to assign the corresponding ν(CO) vibration to the low wavenumber component.[16] Using their results in our case, the 2171−2169 cm^{-1} band is assigned to CO interacting with confined OH_{SP} whereas the 2180−2177 cm^{-1} one is assigned to CO interacting with unconstrained acidic hydroxyls. The possibility for a third ν(CO) component between the 2180−2177 and 2171−2169 cm^{-1} ones was considered, but the broadness and overlapping of bands did not permit any precise conclusion. We thus decided to decompose the ν(CO) vibration band into two main compo-

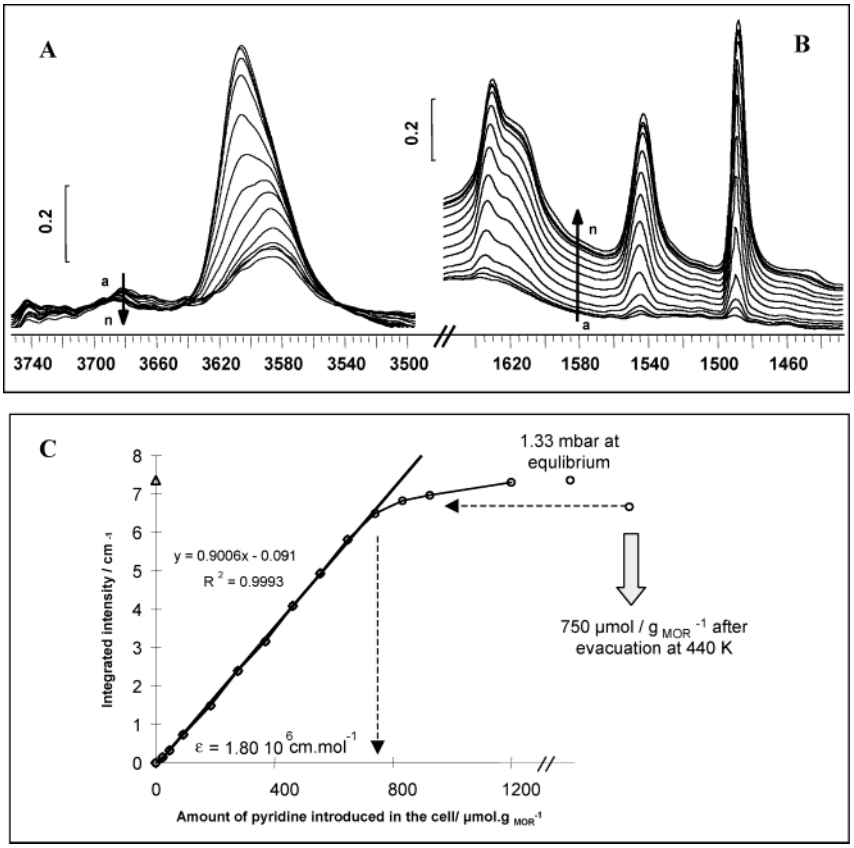

Figure 3. Infrared spectra recorded in the (A) ν(OH) and (B) pyridine cycle vibration regions during adsorption of increasing amounts of pyridine on $H_{97}Na_3MOR$: (a) initial state; after introduction of Py amounts (μmol pyridine/g mordenite) of (b) 23, (c) 46, (d) 92, (e) 185, (f) 278, (g) 370, (h) 463, (i) 555, (j) 648, (k) 741, (l) 833, and (m) 926; (n) 1,33 mbar Py at equilibrium. (C) integrated area of the 1545 cm^{-1} band versus Py amounts introduced into the cell.

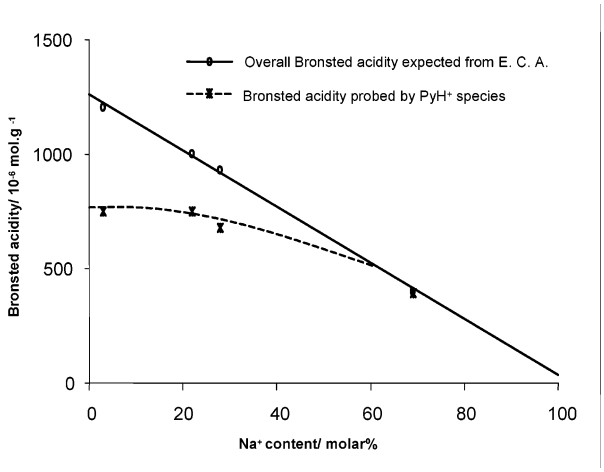

Figure 4. Amounts of Brønsted acid sites estimated from chemical analysis (overall acidity) and from Py adsorption (sites accessible to Py) in the $H_xNa_{100-x}MOR$ samples with increasing Na^+ contents.

nents and since the ϵ(CO) extinction coefficient was reported to be constant in the overall 2200−2150 cm^{-1} range,[38−39] we could quantify the percentages of nonconstrained (2/3) and constrained (1/3) OH groups. Interestingly, the values totally agree with the above estimation of protons accessible (2/3) or not (1/3) to Py.

In the proton-free $H_0Na_{100}MOR$, the first CO doses led to an infrared spectrum with two main ν(CO) components centered at ca. 2181 and 2166 cm^{-1} (Figures 5B, a′ to 5B, d′). These two bands increased in intensity with increasing CO content and progressively shifted to ca. 2174 and 2163 cm^{-1}, respectively (Figure 5B, e′ to 5B, j′). The polarizing effect of the cation

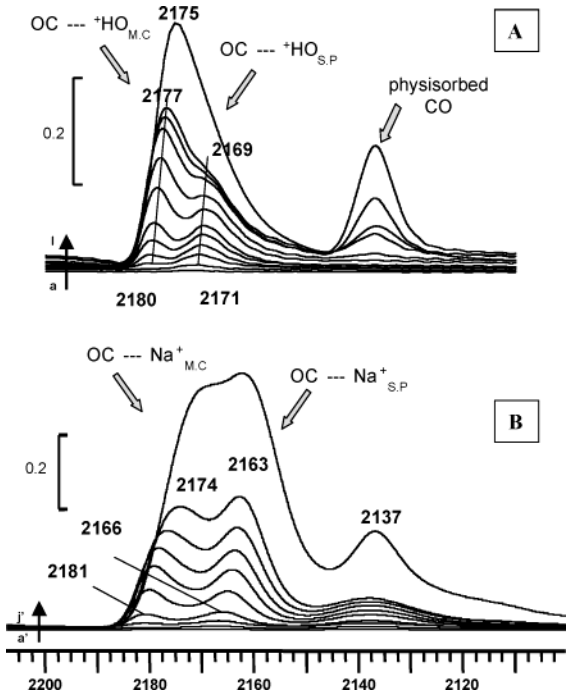

Figure 5. Infrared spectra in the ν(CO) vibration region of (A) $H_{100}Na_0MOR$ and (B) $H_0Na_{100}MOR$ during adsorption at low temperature of increasing amounts of CO equal to (in μmol CO/g mordenite) (a) 36, (b) 72, (c) 144, (d) 216, (e) 287, (f) 359, (g) 485, (h) 610, (i) 736, (j) 862, (k) 988; (a′) 22, (b′) 44, (c′) 88, (d′) 176, (e′) 326, (f′) 457, (g′) 580, (h′) 691, (i′) 803; (l) and (j′) are the spectra at 1.33 mbar equilibrium.

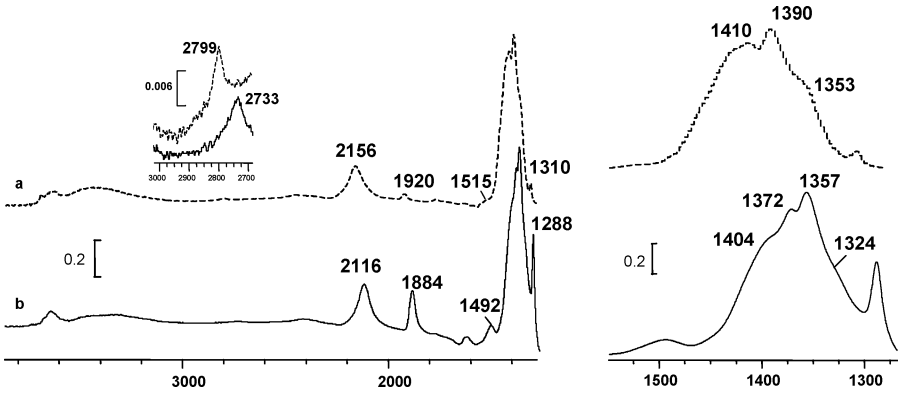

Figure 6. Infrared spectra of H_0Na_{100}MOR after 1 h reaction (room temperature) of nitrogen monoxide and oxygen in initial molar ratio $NO/O_2 = 1$ using (a) ^{14}NO and (b) ^{15}NO. Left: overview of the mid infrared (inset: enlargement of the 3000−2700 cm^{-1} region). Right: nitrates vibration region.

on which the CO probe is adsorbed plays a major role: the higher the polarizing effect, the higher the corresponding ν(CO) wavenumber.[36] It was reported that Na^+ cations in the side pockets of mordenite are shielded by the oxygen atoms on the zeolitic walls, thus polarizing less the CO molecules than in the main channels.[37] Therefore, the 2166−2163 cm^{-1} band can be straightforwardly assigned to Na^+ cations in a constrained environment and that at 2181−2174 cm^{-1} being rather due to cations in the main channels. This assignment is further supported by the fact that the 2181−2174 cm^{-1} band ($\Delta\nu$(CO) = 7 cm^{-1}) is more sensitive to CO coverage than the 2166−2163 cm^{-1} band ($\Delta\nu$(CO) = 3 cm^{-1}), which agrees with the higher amount of CO in the main channels. Similar effects were already reported for mordenite with Si/Al ratio of 5.[36] As previously done for OH groups, we calculated from spectral decomposition (spectrum at 1.33 mbar equilibrium) the proportions of Na^+ cations located in constrained (≅2/3) and nonconstrained (≅1/3) environments. The data are opposite to what was obtained for protons.

3.5. Study of Nitrate Formation. We recently showed that sodium nitrates can form from gas-phase NO and O_2 in the main channels of mordenite but not in the constrained side pockets.[40] To gain more information on the environment and location of Na^+ cations in mordenite, we studied the influence of isotopic labeling on the spectrum of so-formed nitrates and we quantified them on our parent H_0Na_{100}MOR sample (Figure 6).

The species adsorbed after 1 h of reaction between ^{14}NO and O_2 were characterized by an intense band at 2156 cm^{-1} and by a broad and intense band group (doublet at 1410 and 1390 cm^{-1}, with a shoulder at 1353 cm^{-1}) assigned to NO^+ species[40] and to nitrates,[41] respectively. We assigned the very sharp weak band at 2799 cm^{-1} to the combination band of the nitrates vibrations (1410 + 1390 = 2800 cm^{-1}), accordingly with its intensity ratio (1%), which also meant that the 1410 and 1390 cm^{-1} bands originated from the same species. The reaction proposed for nitrate formation is

$$2NO + O_2 + Na^+zeolite^- = NO^+zeolite^- + NaNO_3$$

suggesting that the band at 2156 cm^{-1} is due to NO^+ ions in exchangeable cationic positions. The three additional bands observed at 1920, 1515, and 1310 cm^{-1} were already described as three vibration modes of N_2O_3 adsorbed on Na^+,[41] which is most probably formed from intermediate N_2O_4 gaseous species.[43−44]

We next performed the reaction using ^{15}N labeled NO to confirm the assignments of bands and validate the proposed reaction. The isotopic ratio between the infrared frequencies [$\nu(^{14}NO)/\nu(^{15}NO) = 2156/2116 = 1.019$] was in agreement with NO^+ species being formed.[40] We also compared the observed isotopic shifts with literature data[44] for the 1920, 1515, and 1310 cm^{-1} bands (shift to 1884, 1492, and 1288 cm^{-1} for the ^{15}N-containing species) and confirmed the assignment to N_2O_3. Isotopic shifts on the nitrate bands revealed a complex structure. The isotopic shift of the sharp weak 2799 cm^{-1} band to 2733 cm^{-1} was in good agreement with a combination band for two doublets: 1357 + 1372 = 2729 cm^{-1} and 1404 + 1324 = 2728 cm^{-1}. Each doublet was due to a specific nitrate as pointed out by isotopic shift. The second doublet was much narrower, indicating a much higher ionicity.[45] We thus confirmed the proposed reaction for the formation of nitrates on the surface and pointed out that nitrates exist with two distinct ionicity levels probably related to two distinct unconstrained Na^+ in the MOR structure.

We could then use the reaction equation to quantify the amount of Na^+ cations taking part in the reaction, by a careful monitoring of the gas pressure in the cell during the reaction. Thermodynamic data indicate that NO can react with O_2 to form NO_2 at the temperature and pressure conditions used in our experiments,[46] but we measured a very slow gas-phase reaction (pressure decrease) in the absence of any catalyst in the cell, which permitted to neglect this reaction in the presence of our catalyst. We therefore estimated that the whole pressure decrease was due to adsorption on the zeolite. At equilibrium, between 1510 and 1595 μmol gas phase had disappeared per gram of dry H_0Na_{100}MOR which means, by assuming a low amount of adsorbed N_2O_3 (weak infrared band), that between 500 and 530 μmol $NaNO_3$ were formed per gram of catalyst (three "2NO + O_2" molecules are required to form one $NaNO_3$). Thus, knowing the total Na^+ content from chemical analysis (1300 μmol/g), we could conclude that ≅40% only of the Na^+ ions were able to react with NO + O_2 in proton-free H_0Na_{100}MOR. As we already showed,[40] steric hindrance in the MOR structure inhibits the formation of nitrate species on sodium cations located in the side pockets. Here, unconstrained Na^+ cations thus only account for 40% of the total ion content and lead to two nitrates with distinct ionicities which could indicate the presence of two distinct unconstrained Na^+ sites in the MOR structure.

4. Discussion

4.1. Crystallographic Sites in MOR. The schematic representation of the MOR structure details the different crystallographic sites reported in the literature for tetrahedral (T = Si, Al) atoms, extraframework cations, and oxygen (O) atoms (Figure 7). The four different crystallographic sites for T atoms

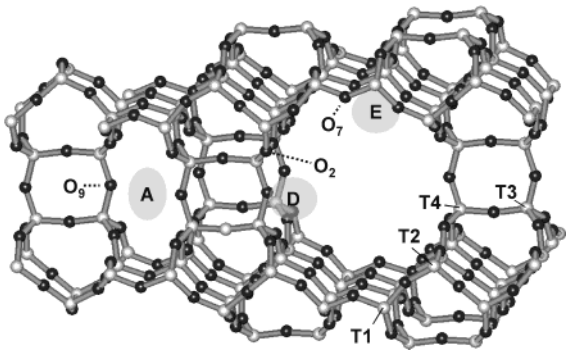

Figure 7. Zeolitic framework of mordenite showing the different crystallographic positions for aluminum atoms (T1−T4), extraframework cations (A, D, and E; from ref 16) and OH location (O2, O7, and O9 from ref 18).

(labeled T1−T4) lead to four possible positions for framework Al atoms, located in the 12-mr main channel (T2 and T4), T3 in the side pockets (T3), and in the 6-mr sheets of the structure, between the 8-mr and 12-mr (T1).[47−48] A unit cell contains 48 T atoms, T1 and T2 being more numerous (16 of each) than T3 and T4 (8 of each).[7,26] Starting from the natural Si/Al ratio (≅5), dealumination treatments can influence the Al distribution between these sites,[48−49] Al atoms being possibly located on the four positions.[49]

The interconnection of the tetrahedral sites through oxygen bridges gives rise to 10 different crystallographic sites for oxygen atoms classically referenced to as O1−O10.[26,51] Only part of these different oxygen types can give rise to acidic hydroxyls and generate sites for extraframework exchangeable cations. From a cross-check of spectroscopic and crystallographic data, the framework oxygen atoms labeled as O_2, O_7, and O_9 were proposed as the best candidates for acidic protons holders.[26] In an earlier study, eight different locations (A−H) were described as possible cationic sites in MOR in the compilation of Mortier.[52] Among them, three sites were identified for Na^+ cations in defect-free Na-MOR samples, using TSDC relaxation map analysis.[24] One of the locations was already known since the 1960s,[53] corresponding to the A site (Figure 7) and now denoted as the Na(I) position. This position is right in the side pocket, with important constrains. Small cations are readily blocked in this position, even in hydrated samples, which explains its early XRD detection. Interesting work on dehydrated single crystals indicated that the two other sodium sites are at D and E sites (Figure 7), now denoted as the Na(IV) and Na(VI) sites, respectively.[54] Site D-Na(IV) is at the opening of the side pockets, and site E-Na(VI) is more in the middle of large channels, near to its wall. The relative occupancies of these three Na^+ positions in Na-MOR samples were estimated for samples with Si/Al ratio of 5.5[52,54−55] to be in the following ranges: 43−50% (site A-Na(I)), 32−36% (site D-Na(IV)), and 18−21% (site E-Na(VI)). The higher occupancies of site A-Na(I) and D-Na(IV), located inside and at the entrance of the side pockets, respectively, agree with the fact that the most constrained T3 and T4 sites are the richest in Al atoms.[26]

4.2. Na^+ Sites Occupancies. Our infrared data on parent H_0-Na_{100}MOR show that about two-thirds of the Na^+ cations are in a confined environment, polarizing less the CO molecules than Na^+ cations in the main channels. In agreement, these cations are not able to react with NO + O_2 because of steric constrains which do not permit formation of $NaNO_3$. Then, it is tempting to assume that the other one-third (i.e., ≅33%) unconstrained Na^+ cations are located on the walls of the large main channels, where they can easily interact with the probe and reactant molecules, but this estimation is significantly higher than the Na^+ occupancy reported for sites E-Na(VI) in the main channels (≅20%). This may come from the difference between the Si/Al ratios (Si/Al = 5.5 in the literature vs Si/Al = 11 in our parent Na-mordenite). Dealumination was effectively shown to influence the cationic sites population.[49−50] Nevertheless, our parent Na-mordenite sample was obtained by direct synthesis and it was recently presented that the E-Na(VI) site occupancy measured by thermally simulated current studies always remained below 20% for samples with Si/Al ratios between 5.5 and 12 obtained by direct synthesis.[56] Therefore, it is most probable that some Na^+ cations, possibly located at site D-Na(IV) at the entrance of the side pockets, are also able to form $NaNO_3$ and interact with CO in an unconstrained environment. These unconstrained Na^+ in site D-Na(IV) and those in site E-Na(VI) would thus account for ≅1/3 of the total Na^+ cations. A part of sites D-Na(IV) should then also contribute together with the whole A-Na(I) sites to the high 2/3 (i.e., ≅66%) proportion of constrained Na^+ cations. Therefore, we may assume that slightly different environments of the Na^+ cations may exist in site D, depending on their close oxygen and T atoms neighborhood or content in probe molecule, thus generating changes in the steric constraints at this site which is located at the limit between the main channel and the side pockets.

4.3. OH Groups Occupancies in Acidic MOR. Although three different crystallographic sites were since long described for Na^+ cations in MOR, infrared studies only dealt with two different OH types until very recently.[16,18,57−59] As usually reported for acidic MOR, the ν(OH) spectrum of fully exchanged Na_0H_{100}MOR is broad and it shows the two classical signals of OH_{MC} (3610 cm^{-1} main band) and OH_{SP} (3585 cm^{-1} shoulder), which behaviors in the presence of Py and CO confirm their assignment to sites in unconstrained and constrained environments, respectively. The observation of a third ν(OH) component at 3605 cm^{-1} at intermediate exchange levels, however, reveals that at least a third OH type exists, which was not identified earlier in the ν(OH) spectra of acidic mordenites most probably because of its overlapping with the main bands at high (3610 cm^{-1}) and low (3585 cm^{-1}) wavenumbers.

The presence of a third OH type in MOR was first reported in an NH_3-TPD study of an acidic mordenite (Si/Al = 9.3) in which three different Brønsted acid sites with homogeneous strengths were identified, most probably located in the main channels, at the intersection between main channels and side pockets, and into the side pockets, respectively.[19] Three different OH locations were also used in a recent infrared study to explain the different accessibilities to acidic OH of three nitriles with increasing molecular sizes adsorbed in a commercial acid mordenite (Si/Al = 10).[25] In Alberti's model, established in 1997 on a cross-check of crystallochemical and spectroscopic data, three types of oxygen atoms can bear acidic protons in the structure.[26] In a more recent work using neutron refinements of several mordenites in their deuterated form, they rather concluded to four different OH types,[27] but the thermal treatment they used introduced extraframework phase, which might cause the fourth site.[60] We interpret our results as three possible locations for acidic OH groups in mordenite, thus reporting the first infrared detection of a third OH group in the mordenite structure. In the structure proposed in Figure 7, O_7H and O_2H point toward the center of the main channel, whereas O_9H points toward the center of the side pocket.

4.4. Stepwise Exchange Process and ν(OH) Assignments. The preparation of our series of exchanged mordenite samples

allowed us to follow the progressive replacement of the Na^+ cations by protons and determine the successive sites involved. The ν(OH) vibration band appearing at 3610 cm^{-1} after the first step of exchange (sample $H_{31}Na_{69}MOR$) is typical of OH_{MC} in the main channels and this attribution was confirmed by the full band removal upon Py adsorption. The first Na^+ ions to be removed are the most accessible ones and thus at site E-Na-(VI) close to the wall of the main channels. According to their location, they should give rise after ionic exchange to the acidic hydroxyl O_7H. The first Na^+ ions to be removed are thus at site E, on the wall on the main channels, in line with the preferred location of protons in the main channels, as already known from other works.[57−59,61]

In the next step, sites D-Na(IV), located in the center of the eight-member ring delimiting the entrance of the side pockets, lead to the intermediate O_2H mostly accessible to pyridine. According to its intermediate location between unconstrained and constrained environments, this new acidic hydroxyl is characterized by a ν(OH) band at ca. 3605 cm^{-1} located between the classical bands of unconstrained OH_{MC} (3610 cm^{-1}) and constrained OH_{SP} (3585 cm^{-1}).

According to both Py and CO, these unconstrained O_7H and O_2H sites created first in the exchange process account for two-thirds of all possible OH groups in mordenite. Part of them come from constrained sites D-Na(IV), indicating that one aluminum atom in the mordenite framework can lead to constrained Na^+ cations in the sodium form and to unconstrained OH groups in the acidic form. We want to underline that the OH groups accessible to pyridine include both O_7H giving the band at 3610 cm^{-1} and O_2H (3605 cm^{-1}) because very few of these IR components remained after Py adsorption.

Finally, the most constrained Na^+ ions at site A-Na(I) are removed in the very last step of the exchange process, the 3585 cm^{-1} ν(OH) band of O_9H appearing solely at exchange levels above 75%. Thus, the Na^+ site occupancy in the side pockets would not be higher than 25%, lower than the 43−50% value expected from literature. This 25% value found above for O_9H could be slightly underestimated, because of the small intensities and possible overlapping of infrared bands (in particular bands at 3605 and 3585 cm^{-1}) when these OH groups appear, making any accurate detection of their first formation quite uneasy.

The overall exchange process is summarized in Figure 8, which can be useful for the determination of the cation and OH group locations at a certain exchange level. The diagram is split in three different zones following the crystallographic distribution of sites. To each OH group content (the example is given at 40% OH exchanged) corresponds the complementary Na^+ content (here 60% Na^+). The diagonal line thus follows the exchange process from 100% Na^+ to 100% OH groups. To each point on the diagonal line corresponds a distribution of OH groups (from point A to point B) and of Na^+ ions (from point B to point C). This is, however, only valid for a zeolite structure that has been perfectly preserved, as will be shown in a later paper. The influence of this distribution on the evaluation of the catalytic role of each acid site and how it is affected by the temperature is under current study.

5. Conclusions

Although crystallographic data suggest the presence of three different OH groups in the structure of mordenite, infrared studies only dealt with two different locations of OH groups until very recently: in the side pockets and in the main channels of the pore structure. Two ν(OH) vibration bands were thus identified, at 3610 and 3585 cm^{-1} for OH_{MC} and OH_{SP}, respectively. A careful look at the ν(OH) vibration region in our series of progressively exchanged samples suggests the presence of a third component at 3605 cm^{-1}. A drastic increase was noticed for the molar absorption coefficient when a significant amount of OH_{SP} started to appear.

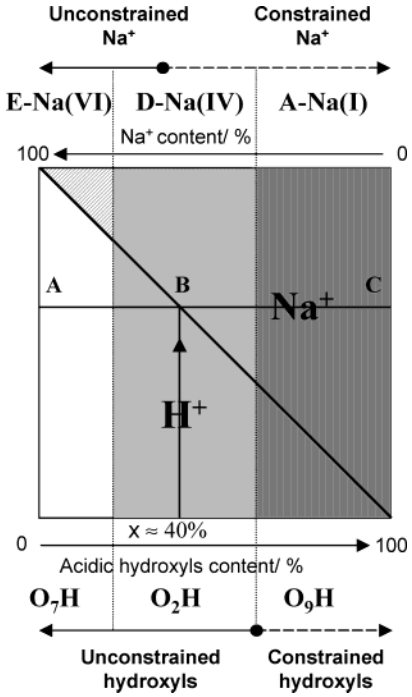

Figure 8. Scheme showing the distribution of sodium cations and acidic hydroxyls over the various sites available inside mordenite.

Pyridine can be used to distinguish the sites in the structure on the basis of accessibility and confinement. Py can only be protonated by unconstrained OH groups, on the conditions that the crystallinity of the sample is perfectly maintained by a gentle thermal treatment. We were able to perturb a large amount of hydroxyls with Py and to quantify these unconstrained sites. They account for two-thirds of all possible OH groups in mordenite and are created first in the exchange process. These results were confirmed by CO adsorption at low temperature. CO was also used for the study of the location of Na^+ cations in the sodium form of the zeolite. Whereas the unconstrained/constrained ratio for OH groups was 2:1 in the acidic zeolite, it was 1:2 for the cations in the sodium zeolite. This suggests that some aluminum atoms lead to constrained Na^+ cations in the sodium form and to unconstrained OH groups in the acidic form. Nitrate formation from NO + O_2 is only possible at unconstrained Na^+ ions in mordenite. On $H_0Na_{100}MOR$, it only involved 40% of the total ion content, and two different types of nitrates were formed.

We propose a model for the progressive exchange of $H_0Na_{100}MOR$ taking into account the three cation sites in the structure, leading to three types of OH groups in the pores. The first hydroxyl group is formed in the main channel (O_7H at 3610 cm^{-1}), the second intermediate one at the opening window between main channels and side pockets (O_2H at 3605 cm^{-1}), and the last created one lies at the end of the side pocket (O_9H at 3585 cm^{-1}). These three OH groups can be distinguished by the combined use of infrared probe molecules, on the condition that the crystalline structure of the zeolite is preserved by a thorough thermal treatment.

References and Notes

(1) Terlouw, T.; Gilson, J. P. *Shell Int. Res. Mij. B. V.* **1991**, EP n° 458 378.

(2) Fellmann, J. D.; Saxton, R. J.; Wentrcek, P. R.; Derouane, E. G.; Massiani, P. *PCT Int. Appl*. 1990; 61 pp.
(3) Sie, S. T.; De Vries, A. F.; Mesters, C. M. A. M.; Boon, A. Q. M.; Bottenberg, K.; Trautrims, B. *Erdoel Erdgas Kohle* **1996**, *112*(11), 463.
(4) Maxwell, I. E.; Stork, W. H. *J. Stud. Surf. Sci. Catal.* **2001**, *137*, 747.
(5) Travers, C.; Raatz, F.; Marcilly, C.; Ramoa, F. R.; Ribeiro, M. F. G. *Eur. Pat. Appl.* 1990; 9 pp.
(6) Corma, A. *Zeolites in oil refining and petrochemistry*; NATO ASI Series, Series C: Mathematical and Physical Sciences, 352 (Zeolite Microporous Solids: Synth., Struct., React.), 1992; p 373.
(7) Baerlocher, C.; Meier, W. M.; Olson, D. H. *Atlas of zeolite structure types*, 5th revised ed.; Elsevier: 2001.
(8) Zecchina, A.; Marchese, L.; Bordiga, S.; Pazè, C.; Gianotti, E. *J. Phys. Chem. B* **1997**, *101*, 10128.
(9) Smirnov, K. S.; Thibault-Starzyk, F. *J. Phys. Chem. B* **1999**, *103*, 8595.
(10) Marie, O.; Thibault-Starzyk, F.; Lavalley, J. C. *Phys. Chem. Chem. Phys.* **2000**, *2*, 5341.
(11) Cartraud, P.; Cointot, A.; Dufour, M.; Gnep, N. S.; Guisnet, M.; Joly, G.; Tejada, J. *Appl. Catal.* **1986**, *21*, 85.
(12) Thibault-Starzyk, F.; Travert, A.; Saussey, J.; Lavalley, J. C. *Top. Catal*. **1998**, *6*, 111.
(13) Bankos, I.; Klyachko, A. L.; Brueva, T. R.; Kapustin, G. I. *React. Kinet. Catal. Lett.* **1986**, *30*(2), 297.
(14) Marie, O.; Thibault-Starzyk, F.; Massiani, P.; Lavalley, J. C. *Stud. Surf. Sci. Catal.* **2001**, *135*, 220.
(15) Ratnasamy, P.; Sivasanker, S.; Vishnoi, S. *J. Catal*. **1981**, *69*(2), 428.
(16) Maache, M.; Janin, A.; Lavalley, J. C.; Benazzi, E. *Zeolites* **1995**, *15*, 507.
(17) Datka, J.; Gil, B.; Kubacka, A. *Zeolites* **1996**, *17*, 428.
(18) Zholobenko, V.; Makarova, M. A.; Dwyer, J. *J. Phys. Chem*. **1993**, *97*, 5962.
(19) Zhiyuan, X.; Leiming, Z.; Quanzhi, L.; Ruiming, Z. *Stud. Surf. Sci. Catal*. **1998**, *49A*, 651.
(20) Karge, H. G.; Dondur, V. *J. Phys. Chem.* **1990**, *94*(2), 765.
(21) Makarova, M. A.; Wilson, A. E.; van Liemt, B. J.; Mesters, C. M. A. M.; de Winter, A. W.; Williams, C. *J. Catal*. **1997**, *172*, 170.
(22) Jacobs, A.; Mortier, W. J. *Zeolites* **1982**, *2*, 226.
(23) Bonn, M.; Bakker, H. J.; Domen, K.; Hirose, C.; Kleyn, A. W.; van Santen, R. A. *Catal. Rev. Sci. Eng.* **1998**, *40*(1&2), 127.
(24) Devautour, S.; Henn, F.; Giuntini, J. C.; Zanchetta, J. V.; Vanderschueren, J. *Solid State Ionics* **1999**, *122*, 105.
(25) Bevilacqua, M.; Busca, G. *Catal. Commun.* **2002**, *3*, 497.
(26) Alberti, A. *Zeolites* **1997**, *19*, 411.
(27) Martucci, A.; Cruciani, G.; Alberti, A.; Ritter, C.; Ciambelli, P.; Rapacciuolo, M. *Microporous Mesoporous Mater.* **2000**, *35*−*36*, 405.
(28) Goovaerts, F.; Vansant, E. F.; De Hulsters, P.; Gelan, J. *J. Chem. Soc., Faraday Trans. 1* **1989**, *85*, 3687.
(29) Thibault-Starzyk, F.; Gil, B.; Aiello, S.; Chevreau, T.; Gilson, J.-P. *Microporous Mesoporous Mater.* **2004**, *67*, 107.
(30) Cannings, F. R. *J. Phys. Chem*. **1968**, *72*, 4691.
(31) Lefrançois, M.; Malbois, G. *J. Catal*. **1971**, *20*, 350.
(32) Buzzoni, R.; Bordiga, S.; Ricchiardi, G.; Lamberti, C.; Zecchina, A.; Bellussi, G. *Langmuir* **1996**, *12*, 930.
(33) Barzetti, T.; Selli, E.; Moscotti, D.; Forni, L. *J. Chem. Soc., Faraday Trans.* **1996**, *92*, 1401.
(34) Kojima, M.; Rautenbach, M. W.; O'Connor, C. T. *J. Catal*. **1988**, *112*, 495.
(35) Khabtou, S.; Chevreau, T.; Lavalley, J. C. *Microporous Mater*. **1994**, *3*, 133.
(36) Bordiga, S.; Lamberti, C.; Geobaldo, F.; Zecchina, A.; Turnes Palomino, G.; Otero Arean, C. *Langmuir* **1995**, *11*, 527.
(37) Zecchina, A.; Bordiga, S.; Spoto, G.; Scarano, D.; Petrini, G.; Leofanti, G.; Padovan, M.; Otero Arean, C. *J. Chem. Soc., Faraday Trans*. **1992**, *88*, 2959.
(38) Zecchina, A.; Scarano, D.; Garrone, E. *Surf. Sci*. **1985**, *160*, 492.
(39) Escalona Platero, E.; Scarano, D.; Spoto, G.; Zecchina, A. *Faraday Discuss. Chem. Soc.* **1985**, *80*, 183.
(40) Henriquès, C.; Marie, O.; Thibault-Starzyk, F.; Lavalley, J. C. *Microporous Mesoporous Mater*. **2001**, *50*, 167.
(41) Chao, C. C.; Lunsford, J. *J. Am. Chem. Soc.* **1971**, *93*, 71.
(42) Katoh, M.; Yamazaki, T.; Kamijo, H.; Ozawa, S. *Zeolites* **1995**, *15*, 591.
(43) Sultana, A.; Loenders, R.; Monticelli, O.; Kirschhock, C.; Jacobs, P. A.; Martens, J. A. *Angew. Chem., Int. Ed.* **2000**, *39*, 2934.
(44) Devlin, J. P.; Hisatsune, I. C. *Spectrochim. Acta* **1961**, *17*, 218.
(45) Laane Ohlsen, J. R. *Prog. Inorg. Chem.* **1980**, *27*, 481.
(46) Chase, M. W., Jr.; Davies, C. A.; Downey, J. R., Jr.; Frurip, D. J.; McDonald, R. A.; Syverud, A. N. *JANAF Thermodynamical Tables*, 3rd ed., vol. 14, suppl. 1; 1985; p 1533.
(47) Olson, R. W.; Rollman, L. D. *Inorg. Chem*. **1977**, *16*, 651.
(48) Bodart, P.; Nagy, J. B.; Debros, G.; Gabelica, Z.; Jacobs, P. A. *J. Phys. Chem.* **1986**, *90*, 5183.
(49) Takaishi, T.; Kato, M.; Itabashi, K. *Zeolites* **1995**, *15*, 21.
(50) Itabashi, K.; Fukushima, T.; Igawa, K. *Zeolites* **1986**, *6*, 30.
(51) Demuth, T.; Hafner, J.; Benco, L.; Toulhouat, H. *J. Phys. Chem*. **2000**, *104*, 4593.
(52) Mortier, W. J. *Compilation of Extraframework Sites in Zeolites*; Butterworth Scientific Ltd.: Guildford, Surrey, U.K., 1982.
(53) Meier, W. M.; *Z. Kristallogr.* **1961**, *115*, 439.
(54) Schlenker, J. L.; Pluth, J. J.; Smith, J. V. *Mater. Res. Bull*. **1979**, *4*, 751.
(55) Coughlan, B.; Caroll, W. M.; McCann, W. A. *J. Chem. Soc., Faraday Trans.* **1977**, *73*, 1612.
(56) Pamba, G.; Maurin, S.; Devautour, J.; Vanderschueren, J.; Giuntini, C.; Di Renzo, F.; Hamidi, F. *Phys. Chem. Chem. Phys.* **2000**, *2*, 2027.
(57) Datka, J.; Gil, B.; Kubacka, A. *Zeolites* **1995**, *15*, 501.
(58) Datka, J.; Gil, B.; Kubacka, A. *Zeolites* **1997**, *18*, 245.
(59) Datka, J.; Gil, B.; Brunner, E.; Koch, M.; Staudte, B. *Bull. Polish Academ. Sci. Chem*. **1997**, *45*, 161.
(60) Fritz, P. O.; Lunsford, J. H. *J. Catal*. **1989**, *118*, 85.
(61) Moreau, F.; Ayrault, P.; Gnep, N. S.; Lacombe, S.; Merlen, E.; Guisnet, M. *Microporous Mesoporous Mater*. **2002**, *51*, 211.